Available online at www.sciencedirect.com
SCIENCE DIRECT®
International Journal of Hydrogen Energy 30 (2005) 1437–1446
International Journal of HYDROGEN ENERGY
www.elsevier.com/locate/ijhydene

Experimental and theoretical analysis of hydrogen absorption in $LaNi_5$–H_2 reactors

A. Demircan[a], M. Demiralp[b], Y. Kaplan[b,*], M.D. Mat[b], T.N. Veziroglu[c]

[a]*Department of Chemistry, Nigde University, 51100 Nigde, Turkey*
[b]*Mechanical Engineering Department, Nigde University, 51100 Nigde, Turkey*
[c]*Clean Energy Research Institute, University of Miami, Coral Gables, FL 33124, USA*

Available online 23 March 2005

Abstract

Hydrogen absorption in two $LaNi_5$–H_2 reactors is experimentally and theoretically investigated. In the experimental program, two tanks are filled with $LaNi_5$ alloy and hydrogen is charged with a constant pressure. The temperature changes in the tanks are measured at several locations and recorded in a computer. Hydriding process is identified from measured temperature histories.

In the theoretical program, a two-dimensional mathematical model, which considers complex heat and mass transfer and fluid flow is developed and numerically solved. The numerical results are compared with the measured data to validate the mathematical model. A reasonable agreement between the numerical results and experimental data is obtained.

Keywords: Hydrogen storage; $LaNi_5$ hydride; Heat and mass transfer; Mathematical model

1. Introduction

Hydrogen energy is the best alternative to fossil fuels due to its high calorific value and being environmentally friendly. Hydrogen also produces more energy per unit weight than any other fuel. However, storage problem of hydrogen prevents its wide usage and commercialization.

Low density of hydrogen creates several storage problems such as high pressure and large volume requirements, weight and safety risks. Some intermetallic compounds, have been found to absorb and release relatively large amounts of hydrogen rapidly at a relatively low pressure; therefore they are under consideration as a practical means of storing hydrogen. Thus, the metal-hydride reactors lead the scientists to focus on rare metal alloys that have several advantages including reversibility of absorption/desorption, unit volume of metal hydride holds, low-pressure equipment, safety implication and little energy requirements.

As far as chemical storage in metal alloys in the form of metal hydrides is concerned, there has been great interest on many metals such as Mg, Na, La, Li etc. [1–5]. The critical issues for storage materials are amount of hydrogen absorbed/desorbed, thermal stability of the hydride, hydrating/dehydrating kinetics, thermodynamic and thermophysical properties, crystal structures, surface processes like segregation, carbonization. Therefore, efficient conditions to form metal alloys has been the main target for chemists, metallurgist, and engineers (Table 1).

Due to the high hydrogen storage capacity, relatively low working temperature and pressure, $LaNi_5$ was chosen for our initial experimental work. Lanthanum and nickel seem to be the most promising alloys, from the aspects of great number of hydrating/dehydrating cycle capacity and physicochemical characteristics, such as unchanged particle size,

* Corresponding author. Tel.: +90 388 225 2249; fax: +90 388 225 0112.
E-mail address: ykaplan@nigde.edu.tr (Y. Kaplan).

0360-3199/$30.00
doi:10.1016/j.ijhydene.2005.02.002

Nomenclature

C_p	specific heat, $J\,kg^{-1}\,K^{-1}$
E_a	activation energy, $J\,mol^{-1}$
h	heat transfer coefficient, $W\,m^{-2}\,K^{-1}$
H	reactor height, m
H/M	hydrogen and metal atomic ratio,
$\dot{m}$	hydrogen mass absorbed, $kg\,m^{-3}\,s^{-1}$
P	pressure, Pa
r	radial coordinate, m
r_0	radius of hydride bed, m
R	universal gas constant, $J\,mol^{-1}\,K^{-1}$
t	time, s
T	temperature, K
u	velocity, $m\,s^{-1}$
z	axial coordinate, m

Greek letters

ΔH^0	reaction heat of formation, $J\,kg^{-1}$
ε	porosity,
λ	thermal conductivity, $W\,m^{-1}\,K^{-1}$
μ	dynamic viscosity, $kg\,m^{-1}\,s^{-1}$
ρ	density, $kg\,m^{-3}$
ϕ	generic variable that representing the variable solved, (i.e., u, v, T)
Γ	exchange coefficient

Subscripts

e	effective
eq	equilibrium
f	cooling fluid
g	gas
0	initial
s	solid
ss	saturated

Table 1
Thermophysical properties of materials and data used in computations

	Metal ($LaNi_5$)	Hydrogen
Density, ρ ($kg\,m^{-3}$)	8200 Ref. [14]	:0.0838 Ref. [15]
Specific heat, C_p ($J\,Kg^{-1}\,K^{-1}$)	:419 Ref. [14]	:1489 Ref. [15]
Thermal conductivity, λ ($W\,m^{-1}\,K^{-1}$)	:1.2 Ref. [14]	:0.12 Ref. [15]
Inlet temperature of gas, (T_0)	:293 K	
Initial temperature of bed and wall, (T_f)	:293 K	

phase composition and processing at low temperatures. Recent reports have opened up a new field of research whether to use or not mish-metal like Co, Ti. Non-hydridible mish-metals make the hydride properties more stable by reducing the hydrating/dehydrating capacity.

Developments in metal-hydride technology show that metal hydrides provide opportunity for hydrogen storage to a high standard of safety both mobile and stationary applications.

There are continuous efforts to enhance properties of hydriding alloys. Addition of other alloying materials significantly changes the working temperature of the La–Ni system. Using La–Ni–Al system as hydrogen absorbing alloy, Asakuma et al. [4] performed experiments from −80 °C to +140 °C and from 10^{-6} to 100 bar. Argon, helium and nitrogen gases were used as the filling gases. Thermal conductivity of the metal-hydride bed is analyzed by the homogenization method using multi-scale alloy; specifically changing contact area of hydrogen with metal surface, Asakuma et al. [4] also developed a model for prediction of thermal conductivity in such system. However, the value of conductivity calculated with the model overpredicts the measured one at high pressure. They indicate that differences between their experimental data and results at high pressure are caused by the assumption that the hydride bed is expressed by the simple cell model, which has the minimum contact points between particles and the minimum surface area between particles and gas.

It is experimentally found that addition of some organic and inorganic materials enhance the hydriding process. Güvendiren and Öztürk [9] analyzed the effects of additives on mechanical milling and hydrogenation of magnesium. Some substances like graphite and Al_2O_3 are the most effective additives for the hydrogen absorption for the magnesium powder, which accelerate the absorption capacity to 6.0 wt%.

Chi and his co-workers performed mechanical ball milling with benzene [2]. They indicated that the ball milling in a a-polar organic solvent offers a new way for magnesium-based hydrogen storage materials, exploiting their higher capacity and higher equilibrium pressure while operating at lower temperature. Results show that there are obvious

differences in the surface morphology for different ball milling conditions [2].

Theoretical studies also shed light on hydriding process and much useful information is obtained. Sun et al. [1], Choi and Mills [5], Ben Nasrallah and co-workers [6–8], Mat and co-workers [10–13] developed several mathematical models for detailed analysis of metal-hydride bed operations.

Jemni and Nasrallah [6] developed two mathematical models, one based on solid and gaseous phase and the other considers solid and gaseous phases as a mixture. Based on Jemni and Nasrallah's continuum mixture model, Mat and co-workers [10–13] carried out a detailed analysis and studied the parameters effecting the hydriding process, and extended the analysis to three-dimensional cases. A prediction of heat and mass transfer in a closed metal hydrogen reactor is based on mathematical and numeric model, besides, the measured evolutions of pressure in the reservoir, which was reported by Askri et al. [8]. This study contains development of a theoretical model that makes it possible to predict the transient heat and mass transfer in a closed cylindrical reactor. They also discuss some governing operating conditions such as gaseous part volume, height to the radius ratio of the reactor and the initial hydrogen to metal atomic ratio, and temperature.

Although there are several theoretical and experimental studies in the literature on the various aspects of the hydrogen storage processes, there are very limited studies validating theoretical models and investigating various bed geometries on hydriding process. Therefore, the objective of this study is to study theoretically and experimentally hydrogen absorption in metal-hydride reactors and analyze various bed geometries and configurations in order to reduce the storage time.

2. Mathematical model

Metal hydride formation is considered in two-dimensional metal-hydride reactors shown in Fig. 1a and b. Two different reactors were designed for experiments. The first reactor is a cylindrical tank with 40 mm radius and 120 mm height (Fig. 1a). The second reactor consists of two co-eccentric cylinders and the space between the cylinders is used as a bed (Fig. 1b). The inner radius of the bed is 20 mm while outer radius and height were calculated as 40 and 160 mm, respectively, in order to have some volume with the first reactor.

The differential equations governing the hydriding process are mass balance of hydrogen and metal, and momentum and energy equations [10].

Mass balance for hydrogen

$$\varepsilon\frac{\partial\rho_g}{\partial t}+\frac{1}{r}\frac{\partial}{\partial r}(r\rho_g u_r)+\frac{\partial}{\partial z}(\rho_g u_z)=-\dot{m}. \tag{1}$$

Mass balance for metal

$$(1-\varepsilon)\frac{\partial\rho_s}{\partial t}=\dot{m}. \tag{2}$$

Momentum equations

in r-direction

$$\rho\frac{\partial u_r}{\partial t}=-\frac{\partial p}{\partial r}+\mu\left(\frac{\partial}{\partial r}\left(\frac{1}{r}\frac{\partial}{\partial r}(ru_r)\right)+\frac{\partial^2 u_r}{\partial z^2}\right)-\rho\left(u_r\frac{\partial u_r}{\partial r}+u_z\frac{\partial u_r}{\partial z}\right)+S_D \tag{3}$$

in z-direction

$$\rho\frac{\partial u_z}{\partial t}=-\frac{\partial p}{\partial z}+\mu\left(\frac{1}{r}\frac{\partial}{\partial r}\left(r\frac{\partial u_z}{\partial r}\right)+\frac{\partial^2 u_z}{\partial z^2}\right)-\rho\left(u_r\frac{\partial u_z}{\partial r}+u_z\frac{\partial u_z}{\partial z}\right)+S_D, \tag{4}$$

where S_D is a source term representing the flow in porous medium and is derived from Darcy's law as

$$S_D=-\frac{\mu}{K}\vec{u}, \tag{5}$$

where K is the permeability of the porous medium.

Energy equation

For the fluid

$$\varepsilon\rho_g C_{pg}\frac{\partial T_g}{\partial t}=\frac{1}{r}\frac{\partial}{\partial r}\left(\varepsilon r\lambda_{ge}\frac{\partial T_g}{\partial r}\right)+\frac{\partial}{\partial z}\left(\varepsilon\lambda_{ge}\frac{\partial T_g}{\partial z}\right)-(\rho_g C_{pg}u_r)\frac{\partial T_g}{\partial r}-(\rho_g C_{pg}u_z)\frac{\partial T_g}{\partial z}-h_{gs}(T_g-T_s)-\max(-m,0)C_{pg}(T_g-T_s). \tag{6}$$

For the solid

$$(1-\varepsilon)\rho_s C_{ps}\frac{\partial T_s}{\partial t}=\frac{1}{r}\frac{\partial}{\partial r}\left((1-\varepsilon)r\lambda_{se}\frac{\partial T_s}{\partial r}\right)+\frac{\partial}{\partial z}((1-\varepsilon)\lambda_{se})\frac{\partial T_s}{\partial z}+h_{gs}(T_g-T_s)+\dot{m}(\Delta H^0+C_{ps}T_s-C_{pg}T_g), \tag{7}$$

where ε is the porosity, u_r and u_z are the velocity components in the r- and z-direction, respectively, and ρ, C_p, λ and $\dot{m}$ are effective density, specific heat, effective thermal conductivity and rate of hydrogen absorption, respectively.

The heat exchange coefficient between solid and gas is written as [7]

$$h_{gs}=\frac{\lambda_g}{d_p}(2+1.1Pr^{1/3}Re^{0.6}), \tag{8}$$

where Pr and Re are Prandtl number and Reynolds number, respectively, and d_p is the particle diameter.

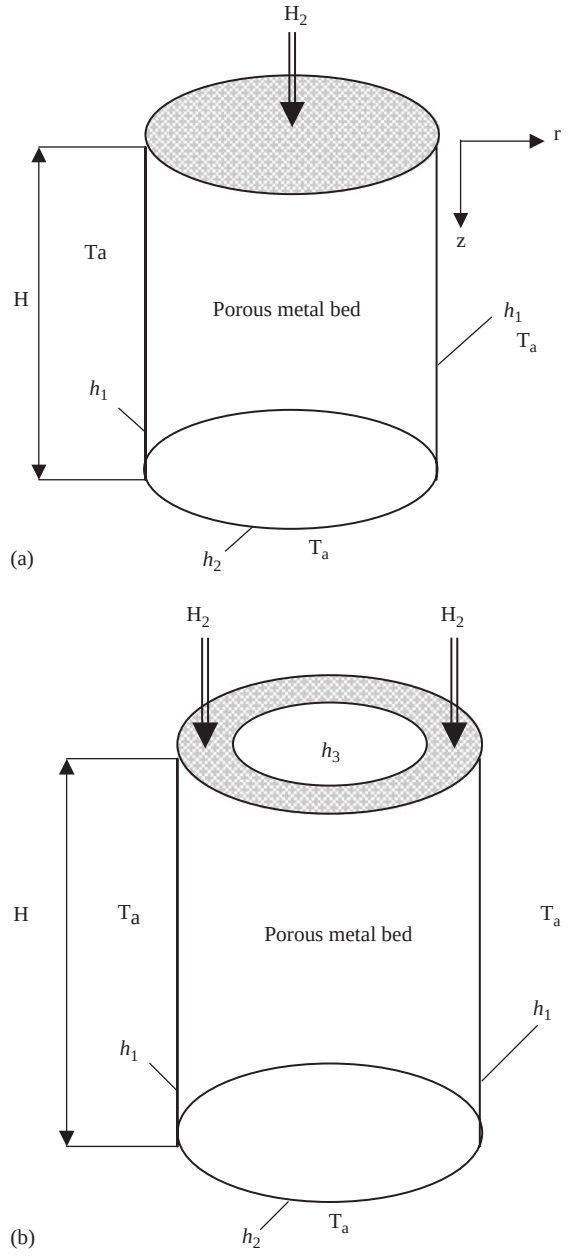

Fig. 1. Schematic sketch of metal-hydride reactors: (a) Reactor I (b) Reactor II.

Auxiliary equations

The amount of hydrogen absorbed is directly linked to the reaction rate, which is expressed as

$$\dot{m} = -C_a \exp\left(-\frac{E_a}{RT}\right) \ln\left(\frac{P_g}{P_{eq}}\right)(\rho_{ss} - \rho_s), \tag{9}$$

where C_a is material-dependent constant, ρ_{ss} is density of the solid phase at saturation and P_{eq} the equilibrium pressure calculated using the van't Hoff relationship

$$\ln P_{eq} = A - B/T, \tag{10}$$

where A and B are materials constants deduced from the experimental data.

Initial and boundary conditions

Initial conditions. Hydrogen charge into metal bed and subsequent hydriding processes in the reactors are shown in Fig. 1a and b. Initially hydride bed is assumed to have constant temperature and pressure and quiescent. These conditions can be expressed mathematically as

$$\text{at } t = 0 \quad P(r, z, 0) = P_0, \quad T(r, z, 0) = T_0, \quad u_r(r, z, 0) = u_z(r, z, 0) = 0. \tag{11}$$

Boundary conditions

Reactor I. The boundary walls are assumed to be impermeable and no slip conditions are valid at the boundary walls. The reaction heat is removed from the boundary walls with a cooling fluid whose temperature is T_f. Hydrogen is charged at $z = 0$ with a constant pressure, P_0 and constant temperature, T_0. The boundary conditions can be expressed as

$$\text{at } r = 0 \quad \frac{\partial T}{\partial r}(0, z, t) = 0, \quad \frac{\partial u}{\partial r}(0, z, t) = \frac{\partial u_z}{\partial r}(0, r, t) = 0, \tag{12}$$

$$\text{at } z = 0 \quad -\lambda\frac{\partial T}{\partial z}(r, 0, t) = h_{gs}(T_0 - T), \quad u_z(r, 0, t) = u_{in}, \tag{13}$$

$$\text{at } r = r_0 \quad -\lambda\frac{\partial T}{\partial r}(r_0, z, t) = h_1(T - T_a), \quad u_r(r_0, z, t) = u_z(r_0, z, t) = 0, \tag{14}$$

$$\text{at } z = H \quad \frac{\partial T}{\partial z}(r, H, t) = h_2(T - T_a), \quad u_r(r, H, t) = u_z(r, H, t) = 0, \tag{15}$$

where h_{gs} is heat transfer coefficient between gas and solid which is calculated from Eq. (8), h_1 and h_2 are the transfer coefficient between solid/air side and its value is calculated from the standard Churchill and Chu equation and the Lloyd and Moran equation [16], respectively.

Reactor II. The second reactor is two co-eccentric cylinders; metal alloy is filled in the space between the cylinders. The boundary conditions for Reactor II can be mathematically summarized as

$$\text{at } z = 0 \quad -\lambda\frac{\partial T}{\partial z}(r, 0, t) = h_{gs}(T_0 - T), \quad u_z(r, 0, t) = u_{in}, \tag{16}$$

$$\text{at } r = r_i \quad -\lambda\frac{\partial T}{\partial r}(r_i, z, t) = h_3(T - T_a), \quad u_r(r_i, z, t) = u_z(r_i, z, t) = 0, \tag{17}$$

$$\text{at } r = r_0 \quad -\lambda\frac{\partial T}{\partial r}(r_0, z, t) = h_1(T - T_a),$$
$$u_r(r_0, z, t) = u_z(r_0, z, t) = 0, \tag{18}$$

$$\text{at } z = H \quad -\lambda\frac{\partial T}{\partial z}(r, H, t) = h_2(T - T_a),$$
$$u_r(r, H, t) = u_z(r, H, t), \tag{19}$$

where h_3 is the heat transfer coefficient in the annulus and calculated using Elenbaas equation [16].

3. Numerical method

The partial differential equations are solved numerically with a fully implicit numerical scheme embodied in PHOENICS code [17]. This code solves the following general differential equation

$$\frac{\partial(\rho\phi)}{\partial t} + \nabla(\rho u\phi) = \nabla(\Gamma\nabla\phi) + S_h, \tag{20}$$

where ϕ is a generic variable representing the variable solved (i.e., u, v, T), Γ is the exchange coefficient. S_h represents the source terms. An important advantage of PHOENICS code is that it allows the user to incorporate additional source term that is not available in the main program.

A 25×60-grid system is employed after a grid refinement test. A typical run until 5000 s takes about 6 h in a Pentium III. PC.

4. Experimental method

Experimental setup for hydrogen absorption is schematically presented in Fig. 2. Setup mainly consists of a reactor, a vacuum pump to evacuate the reactor before the experiment, a ball mill to produce fine particles, manometers, thermocouples, a data acquisition system, a tank containing 99.999% pure hydrogen gas and an argon tank to provide work under inert atmosphere environment. The main objective of the study is to see the effect of heat transfer rate on hydriding time for the two reactors considered.

The following procedure is followed during the experiments:

- $LaNi_5$ material is grounded for 3 h. Grinding procedure is conducted by a ball mill, which is located in a glow box of 60 mm diameter and 80 mm height. Argon gas is used during the process to prevent possible oxidation. Grinding speed was varied between 500 and 890 rpm. During the grinding process, some graphite at a ratio of 1% of $LaNi_5$ is added as an anti-sticking agent. $LaNi_5$ material is used in the experiments.
- Grounded material is transferred into the reactor in a glove box. This process is carried out at argon atmosphere, unless otherwise noted.
- The reactor is heated to almost 200 °C for 2 h under low pressure ($\approx 10^{-4}$ mmHg). After the heating process, the reactor is cooled down to room temperature and then hydrogen is charged to the reactor under 10 bar pressure. These heating and cooling processes are repeated 5 times for activation of $LaNi_5$ alloy.
- The experimental part was started after activation process had completed. Reactors were then charged with hydrogen at a range of pressure (6–10 bars). Hydriding process is monitored with temperature measurements obtained at several locations on the reactor. The temperature readings are recorded on a computer for further processing and interpretation of hydriding behavior.

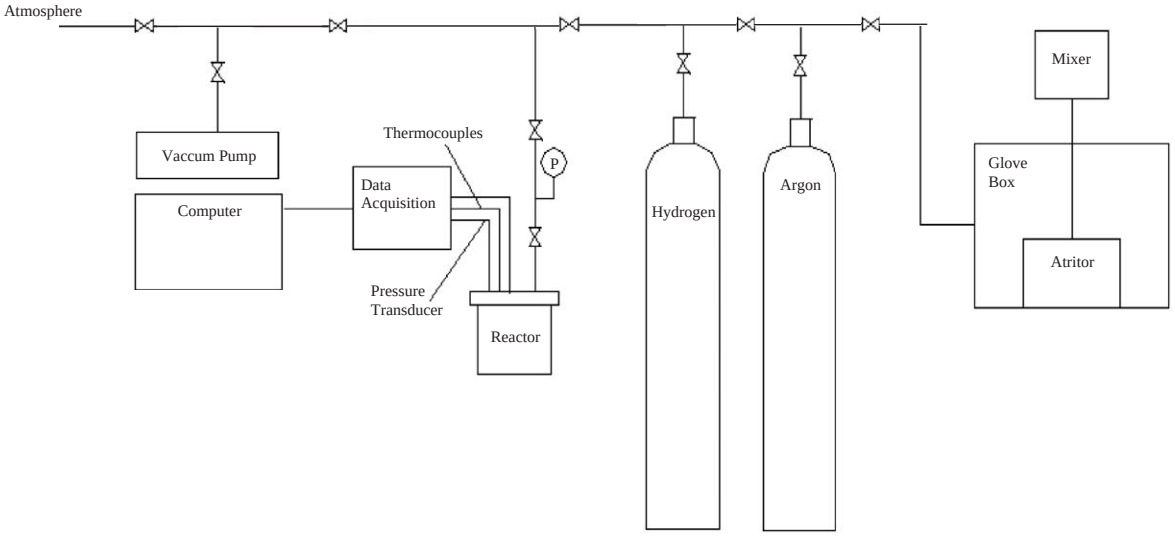

Fig. 2. The experimental setup.

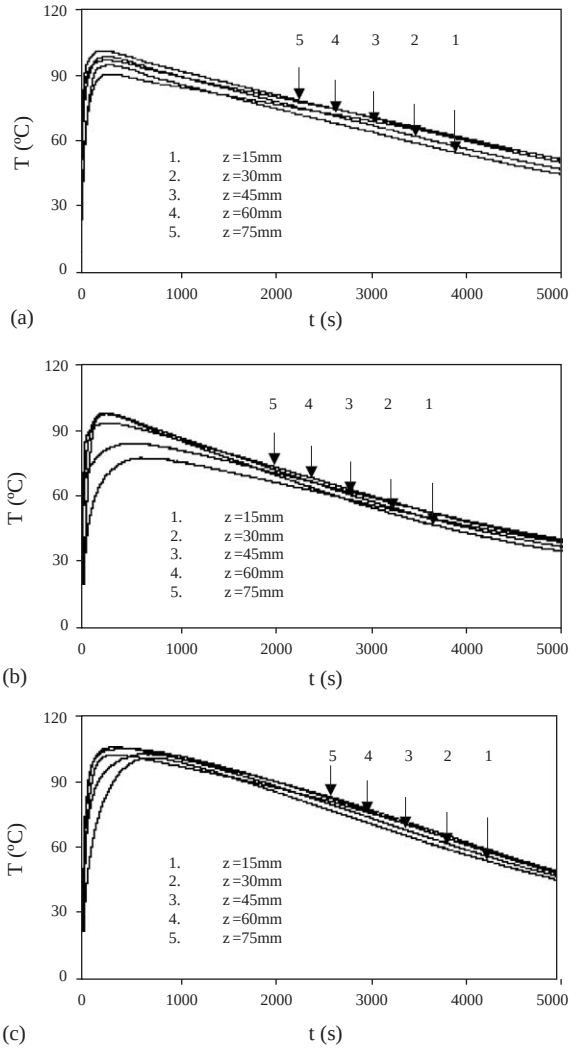

Fig. 3. Measured temperature evolution in Reactor I: (a) 6 bar (b) 8 bar and (c) 10 bar.

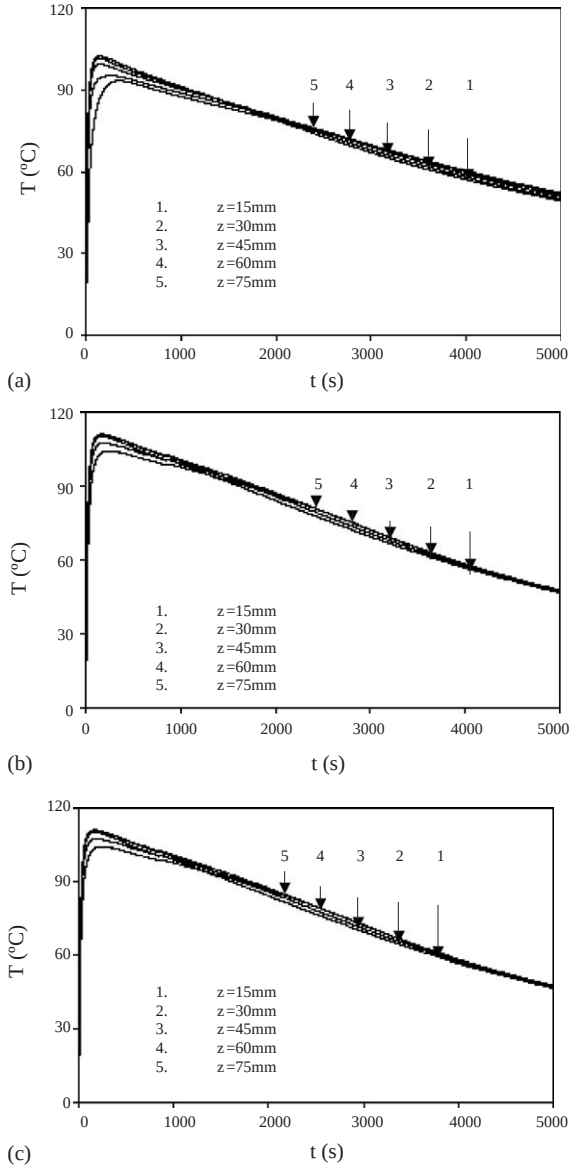

Fig. 4. Measured temperature evolution in Reactor II: (a) 6 bar (b) 8 bar and (c) 10 bar.

5. Results and discussions

The measured temperature evolution in z-direction under several charging pressures within the reactors I and II are given in Figs. 3 and 4, respectively. Experiments are performed under three charge pressures (6, 8 and 10 bars). Temperature changes on the bed are measured at 15, 30, 45, 60, 75 mm from the top of the bed. General characteristic of hydriding process is a sudden increase of bed temperature after charging is initiated. This increase is the result of exothermic hydriding reaction. It is observed that there is a perceivable temperature gradient in the bed within first 500 s in both reactors. This difference vanishes with time in both reactors especially under higher charging pressure (see Figs. 3 and 4). However, a significant temperature gradient observed in Reactor I (Fig. 3). This result may be attributed to the enhanced heat transfer in Reactor II, since hydriding reaction rate is strongly dependent on temperature.

To study hydriding process in detail, we calculated two-dimensional temperature profile and evolution of hydride formation at 100 and 500 s for Reactor I as given in Figs. 5 and 6. It is seen that at around 100 s a sudden increase of bed temperature all over of the bed is evident due to the exothermic hydriding reaction. Temperature near the cooled wall slightly decreases at 500 s. It is seen that H/M (amount of hydride formed/amount of metal) ratio is higher at lower

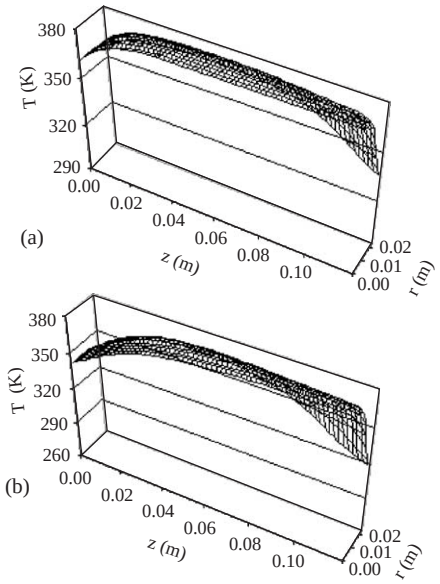

Fig. 5. Temperature profile in Reactor I at selected times: (a) $t = 100$ s (b) $t = 500$ s.

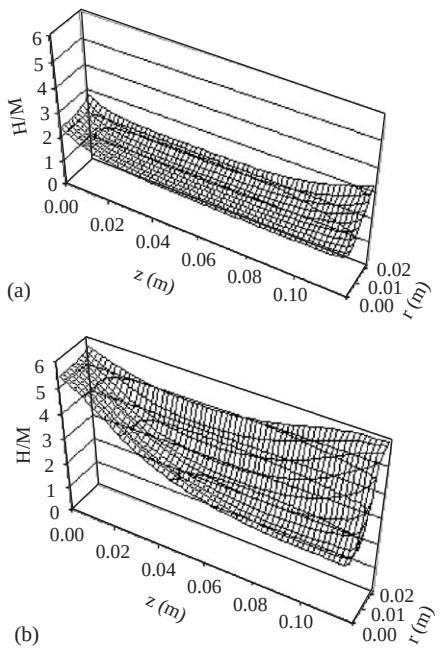

Fig. 6. Evolution of hydride formation in Reactor I: (a) $t = 100$ s (b) $t = 500$ s.

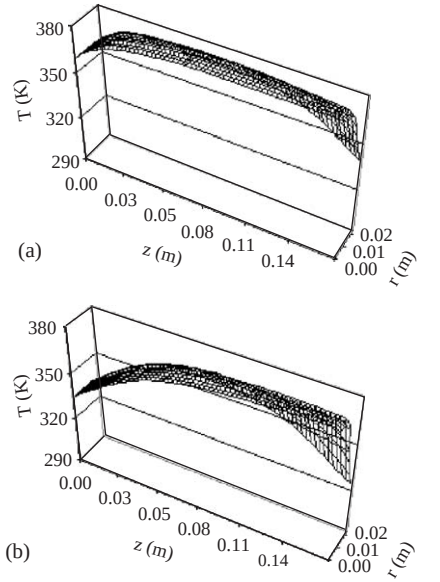

Fig. 7. Temperature profile in Reactor II at selected times: (a) $t = 100$ s (b) $t = 500$ s.

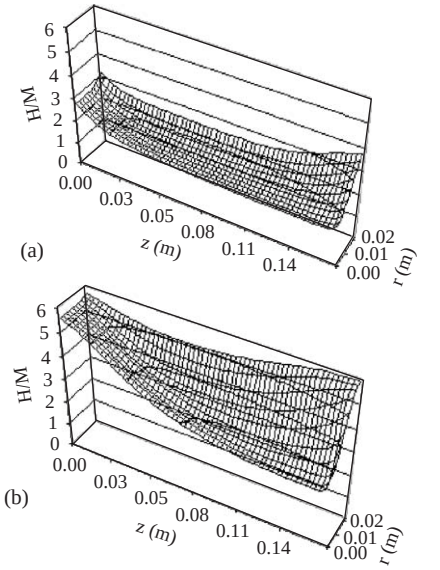

Fig. 8. Evolution of hydride formation in Reactor II: (a) $t = 100$ s (b) $t = 500$ s.

temperatures. Generally more hydride is formed near walls in the z-direction because of cooling effect. There is a gradual decrease in H/M ratio in the middle part of the reactor. This is also true along the radius. Figs. 7 and 8 represent the temperature profile and evolution of hydride formation at same experimental conditions for Reactor II. A similar temperature and H/M distribution is obtained with Reactor II.

Calculated velocity distribution with respect to height and radius of the reactor at 100 and 1500 s are given in Figs. 9 and 10, which are for Reactors I and II, respectively. It

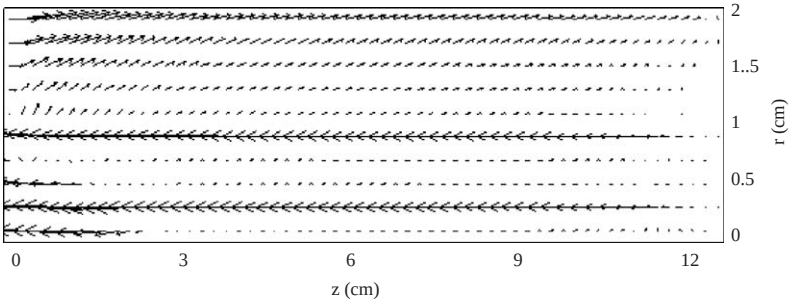

(a) V_{max}=3.91 mm/s

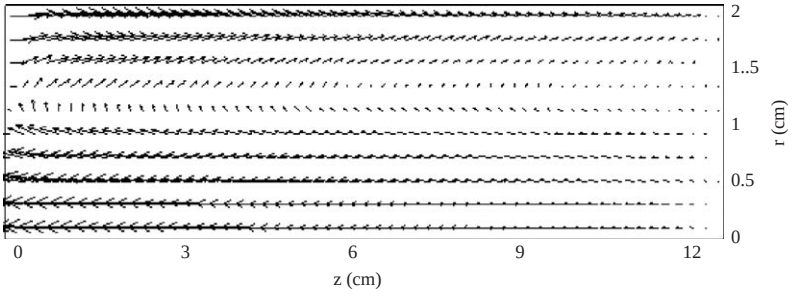

(b) V_{max}=0.0753 mm/s

Fig. 9. Velocity distribution in Reactor I: (a) 100 s (b) 1500 s.

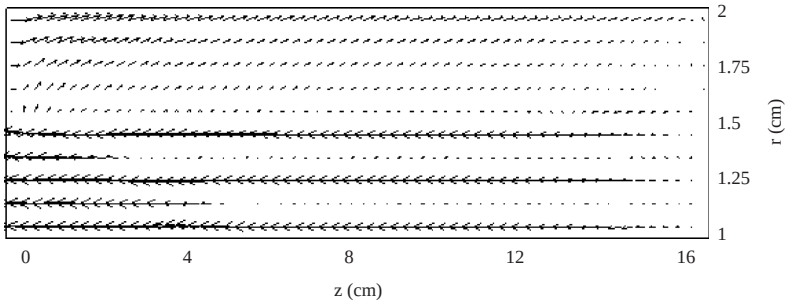

(a) V_{max}=4.14 mm/s

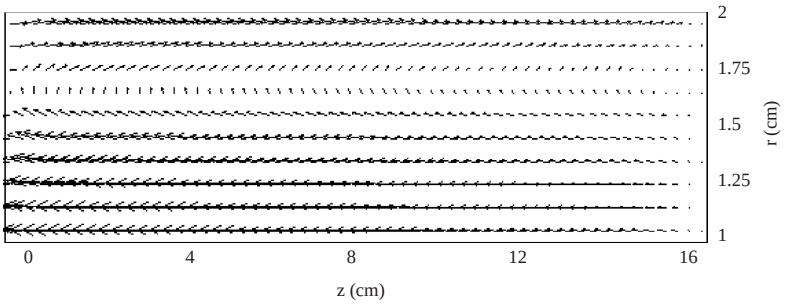

(a) V_{max}=0.0446 mm/s

Fig. 10. Velocity distribution in Reactor II: (a) 100 s (b) 1500 s.

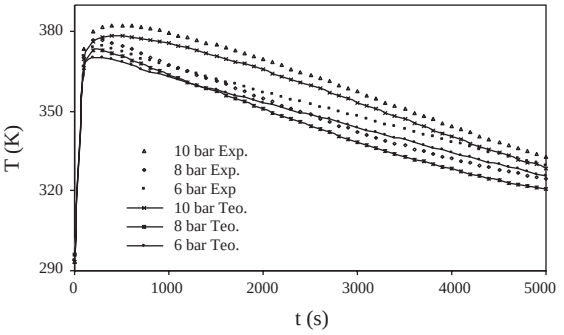

Fig. 11. Influence of the hydrogen gas inlet pressure on the temperature evolution in Reactor I.

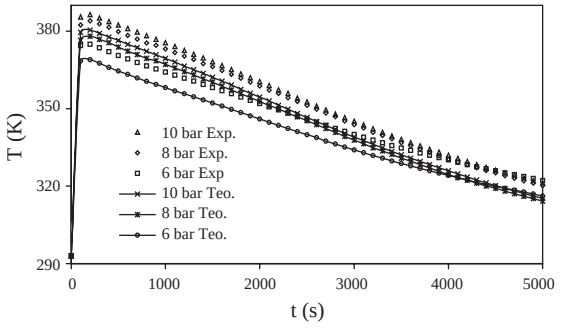

Fig. 12. Influence of the hydrogen gas inlet pressure on the temperature evolution in Reactor II.

is seen that gas velocity is generally higher near the walls of the reactor, which shows good match with temperature profile and H/M ratio that is given above. The main driving mechanics for the flow is the buoyancy generated due to the temperature gradient in the bed. It should be noted that there is a significant drop in velocity with time. Since temperature gradient is decreased at late times, maximum velocities for Reactor II are 4.14 and 0.0446 mm/s at 100 and 1500 s, respectively. It can be concluded that maximum reaction velocity at earlier times is higher in Reactor II when those maximum values are compared with the values obtained for Reactor I, i.e., 3.91 and 0.0753 mm/s at 100 and 1500 s, respectively.

Experimental data and model predictions are compared in Figs. 11 and 12. These figures also reflect the effect of inlet pressure on the hydriding process. The selected inlet hydrogen gas pressures are 6, 8 and 10 bar. There is a slight difference in experimental and theoretical values, which is somehow smaller in Reactor II as compared with Reactor I. It can be seen that evolved temperature values for Reactor II are greater than that of Reactor I. It can be concluded that temperature evolution is very sensitive to hydrogen gas inlet pressure. There is an increase in temperature evolution as the inlet hydrogen pressure increases. This effect is more pronounced between 6 and 8 bar in Reactor I. In Reactor II an higher pressure (10 bar) is needed to see this effect.

6. Conclusion

Hydrogen absorption in metal-hydride reactors is experimentally and theoretically investigated. An experimental setup is designed to study main characteristics of hydriding process and effect of bed geometry and heat transfer on the hydriding process.

Hydriding process is characterized by exothermic reaction between $LaNi_5$ and H_2 and rapid temperature increase due to the heat release. Hydriding time mainly depends on the successful heat removal from the bed. A bed geometry that provides more heat transfer area significantly reduces hydriding time.

A mathematical model is developed to study hydriding process in detail and to study system optimization. Mathematical model considers coupled heat and mass transfer and fluid flow in the hydride bed. The governing equations are numerically solved and calculated results are compared with experimental data. It is found that mathematical model adequately captures the main physics of the hydriding process and can be employed for a better hydride bed design to reduce hydriding time.

Acknowledgements

The authors would like to thank Turkish State Planning Organization (DPT) for the financial support under contract number 2002K120490 and the Scientific and Technical Research Council of Turkey (TUBITAK) through the US–Turkey Cooperative Research Agreement, under contract number MISAG-NSF-13.

References

[1] Sun DW, Deng SJ. A theoretical model predicting the effective thermal conductivity in powdered metal hydride beds. Int J Hydrogen Energy 1990;15(5):331–6.

[2] Chi H, Chen C, Chen L, An Y, Wang Q. Hydriding/dehydriding properties of $LaMg_{16}Ni$ alloy prepared by mechanical ball milling in benzene and under argon. Int J Hydrogen Energy 2004;29:737–41.

[3] Lopez-Suarez A, Rickards J, Trejo-Luna R. Analysis of hydrogen absorption by Ti and Ti-6Al-4V using the ERDA technique. Int J Hydrogen Energy 2003;28:1107–13.

[4] Asakuma Y, Miyauchi S, Yamamoto T, Aoki H, Miura T. Homogenization method for effective thermal conductivity of metal hydride bed. Int J Hydrogen Energy 2004;29:209–16.

[5] Choi H, Mills AF. Heat and mass transfer in metal hydrides beds for head pump applications. Int J Heat Mass Transfer 1990;33(6):1281–8.

[6] Jemni A, Ben Nasrallah S, Lamloumi J. Experimental and theoretical study of a metal-hydrogen reactor. Int J Hydrogen Energy 1999;24(1):631–44.
[7] Jemni A, Ben Nasrallah S. Study of two-dimensional heat and mass transfer during absorption in a metal-hydrogen reactor. Int J Hydrogen Energy 1995;20:43–52.
[8] Askri F, Jemni A, Ben Nasrallah S. Prediction of transient heat and mass transfer in a closed metal-hydrogen reactor. Int J Hydrogen Energy 2004;29:195–208.
[9] Güvendiren M, Baybörü E, Öztürk T. Effect of additives on mechanical milling and hydrogenation of magnesium powders. Int J Hydrogen Energy 2004;29:491–6.
[10] Mat M, Kaplan Y. Numerical study of hydrogen absorption in an $LaNi_5$ hydride reactor. Int J Hydrogen Energy 2001;26(9):957–63.
[11] Kaplan Y, Veziroglu TN. Mathematical modelling of hydrogen storage in a $LaNi_5$ metal-hydride bed. Int J Energy Research 2003;27(11):1027–38.
[12] Mat MD, Kaplan Y, Aldas K. Investigation of three-dimensional heat and mass transfer in a metal hydride reactor. Int J Energy Research 2002;26:973–86.
[13] Aldas K, Mat MD, Kaplan YA. Three dimensional mathematical model for absorption in a metal hydride bed. Int J Hydrogen Energy 2002;27(10):1049–56.
[14] Tragna, DC. Material material data sheet. Ergenic Inc. 2002.
[15] Veziroglu TN, Barbir F. Hydrogen energy technologies. Vienna: UNIDO; 1998.
[16] Incropera FP, DeWitt DP. Fundamentals of heat and mass transfer. 4th ed., New York: Wiley; 1996.
[17] Rosten H, Spalding DB. PHOENICS beginner's guide and user's manual, CHAM Limited (UK). Technical Report, TR/100, 1986.